Supporting Information

Stabilized Four-Electron Aqueous Zinc-Iodine Batteries by Quaternary Ammonium Complexation

Pengjie Jiang[#], Qijun Du[#], Chengjun Lei, Chen Xu, Tingting Liu, Xin He, Xiao Liang*

State Key Laboratory of Chem/Biosensing and Chemometrics, College of Chemistry and Chemical Engineering, Hunan University, Changsha, 410082, P.R. China.
Email: xliang@hnu.edu.cn
# These authors contributed equally to this work.

Experimental

Materials

All reagents were used as received without any further purification. Zinc chloride ($ZnCl_2$), anhydrous zinc sulfate ($ZnSO_4$), hydrogen peroxide (H_2O_2), hydrochloride acid (HCl), dimethylformamide (DMF) and acetonitrile (AN) were purchased from Aladdin. Tetramethylammonium chloride (Me_4NCl), Tetraethylammonium chloride (Et_4NCl), Tetrapropylammonium chloride (Pr_4NCl), Tetrabutylammonium chloride (Bu_4NCl), Tetraamylammonium chloride (Am_4NCl), Tetraheptylammonium Chloride ($Hept_4NCl$), Tetramethylammonium iodide (Me_4NI), Tetraethylammonium iodide (Et_4NI), Tetrapropylammonium iodide (Pr_4NI), Tetrabutylammonium iodide (Bu_4NI), Tetraamylammonium iodide (Am_4NI), Tetrahexylammonium iodide ($Hexy_4NI$) and Tetraheptylammonium iodide ($Hept_4NI$) were purchased from Adamas.

Synthesis of quaternary ammonium dichloroiodate ($QICl_2$)

The quaternary ammonium dichloroiodate could be prepared by two approaches:

$$QCl + IO_3^- + 5\ Cl^- + 6\ H^+ \rightarrow QICl_2 + 3\ H_2O + 2\ Cl_2 \quad (1)$$

$$QI + H_2O_2 + 2\ Cl^- + 2\ H^+ \rightarrow QICl_2 + 2\ H_2O \quad (2)$$

Q means quaternary ammonium cations. For reaction (1), 1 mL 1 M QCl, 1 mL 1

M HIO_3 and 2 mL 36% HCl were stirred in a glass vial for 2 hours. For reaction (2), 1 mmol QI, 5 mL 36% HCl, and 5mL 30% H_2O_2 were stirred in a glass vial and stirred for 2 hours. The precipitates were collected by filtration and washed several times with deionized water to remove unreacted materials. The powder was dried in an oven at 60 °C for 12 h.

Preparation of PAC/I_2

Solution-adsorption method was used for the preparation of PAC/I_2 cathodes. Briefly, 200 mg of I_2 was mixed with 300 mg PAC, followed by adding 25 mL of deionized water. Then, the solution was kept in oven at 60 °C for 12 hours. The dark sample was obtained after filtrating, washing with deionized water and dried at 60 °C for 12 hours successively.

Electrode preparation and cell assembly

The $QICl_2$ electrode was obtained by mixing the synthesized quaternary ammonium dichloroiodate, poly(vinylidene fluoride) (PVDF) and super P in dimethylformamide (DMF) with a mass ratio of 7:2:1. Then the slurry was cast on a titanium foil followed by drying for 12 h in air at 60 °C. The electrodes were cut into disks with a diameter of 12 mm. The average mass loading of the active material in the electrode was 2.0 mg cm^{-2}. The PAC/I_2 electrode was obtained by mixing PAC/I_2, sodium carboxymethyl cellulose and super P in water at a weight ratio of 8:1:1. Then the slurry was cast on a titanium foil followed by drying for 12 h in air at 60 °C. The electrodes were cut into disks with a diameter of 12 mm. The average mass loading in the electrode is 3.0 mg cm^{-2}. Zinc foil with 0.1 mm thickness was used as the anode. Glass fiber was placed between the anode and cathode as the separator. Electrochemical studies were performed in PFA-based Swagelok-type cells (1/2-inch diameter).

Electrochemical measurements

The cells were then galvanostatically charged/discharged on a NEWARE battery test system (Shenzhen, China) at room temperature. The specific capacities of the Zn-I_2 batteries were calculated based on the mass of iodine. The electrochemical impedance

spectroscopy (EIS) was performed on a INTERFACE1010 electrochemical workstation (Gamry, USA) using a 100 μA perturbation with a frequency range of 10 mHz to 1 MHz. Cyclic voltammetry measurements were performed on an electrochemical workstation (Gamry, USA). The GITT test, consisting of a series of current pulses (≈442 mA g^{-1}) for 3 min followed by a 10 min relaxation process, was performed within the voltage range of 0.6 -1.8 V.

Materials characterization.

Raman analyses were carried out on a bench Raman dispersive microspectrometer (InVia Reflex, Renishaw) using a laser (wavelength of 532 nm) at frequencies between 1,500 cm^{-1} and 100 cm^{-1}. For the in-situ Raman test, Raman electrolytic device were employed, the cathode slurry (PAC/I_2 or $Hexy_4NICl_2$ with binder) loaded at a glass carbon electrode followed drying at 60 °C, which is served as the working electrode. The counter electrode is Pt wire and the reference electrode is Ag/AgCl, respectively. UV–vis spectrum characterization was carried out on a UV1902PC with a range from 190 to 600 nm. For the quantify hydrolysis test, equimolar amounts of $QICl_2$ compounds were dispersed/dissolved in water (~ 0.1 M). The solution/suspensions after relaxation were diluted into 0.02 M with acetonitrile and then subjected to UV-vis spectroscopy test. Free ICl is too susceptible hydrolyzed to allow recording of UV-vis results. Thus, its hydrolysis test was changed into introducing 20% vol water into 0.02 M ICl acetonitrile solution, followed by UV-visible spectroscopy monitoring over time. SEM studies were carried out on a Regulus 8100 field-emission SEM instrument. Electrodes were gently washed with deionized water to remove the electrolyte and dried for 6 h in vacuum oven at 40 °C before the characterizations. Thermogravimetric analysis and differential thermal analysis were carried out on a STA7200 thermogravimetric-differential thermal simultaneous analyzer. The sample were dried for 12 h in vacuum oven at 40 °C before the characterizations and test in Argon atmosphere with a heating rate of 10 °C min^{-1}. Solubility was measured as the following steps. In order to prevent the reagents from absorbing water and causing inaccuracy, the reagents was stored in an argon-filled glove box after purchase. After accurately

weighing the required reagents from the glove box into a bottle, it was quickly taken out and add the required water to prepare the solution. The mixture was stirred at 298 K for 12 h and rested for 6 h. Clear solution will be obtained if it was below the saturation solubility, otherwise a suspension or particles could be observed in **Figure 31**.

Calculations

The Gibbs free energy was calculated using density functional theory (DFT) in Gaussian package. The structures were optimized at B3LYP functional with Def2-TZVP/Def2-TZVPD basis set including the atom-pairwise dispersion correction (DFT-D3BJ). The implicit universal solvation model based on SMD18 was applied during the structure optimization. The accurate values of the electronic energy or the solvation free energy for the optimized molecular structures were compute at B2PLYPD3 or M06-2X functional.

The binding energy (E binding) was calculated by the following Eq.

$$E\ binding=E(AB)+E(xH_2O)-E(A+)-E(B-\cdot xH_2O)$$

Where E represents the Gibbs free energy of the component. A represents positive ion and B represents negative ion.

All quantities related to the hydrolysis reaction in the paper were spin polarized and carried out with the PBE functional in DMol3 package. The Grimme-correction method was employed in order to include vdW interactions. Core electrons were replaced by a DFT semi-core pseudopots. For the calculations of total energy, a global orbital cutoff of 4.5 Å was set and the converging criteria of the force on each relaxed atom below 0.002 Ha/Å was used for structural optimizations. The multiple complete LST/QST method was used to find a transition state (TS) when reasonable structures for the reactants and products exist. Those quantities related to the hydrolysis reaction were performed under the COSMO model. In order to improve accuracy and consider a certain degree of solvent effect, the changes of free energy of the following reaction equation are defined as the actual changes of energy during hydrolysis process:

$QICl_2 + H_2O \rightarrow QICl_2 \cdot H_2O \rightarrow TS \rightarrow HIO + HCl + QCl$

For molecular hydrogen chloride and quaternary ammonium chloride, an additional display solvent model was introduced after the last step to obtain the energy change in aqueous solution.

$HCl + 9H_2O \rightarrow Cl^- \cdot 4H_2O + H_3O^+ \cdot 4H_2O$

$QCl + 4H_2O \rightarrow Cl^- \cdot 4H_2O + Q^+$

To obtain the binding strength of anions and cations in the vacuum environment (under anhydrous conditions), the DMol3 software was used to calculate the binding energy and the COSMO model was no longer included in the calculation. The binding energy (E binding) was calculated using the following equation.

E binding=E(AB)-E(A+)-E(B-)

where E is the energy of the component A represents the positive ion and B the negative ion.

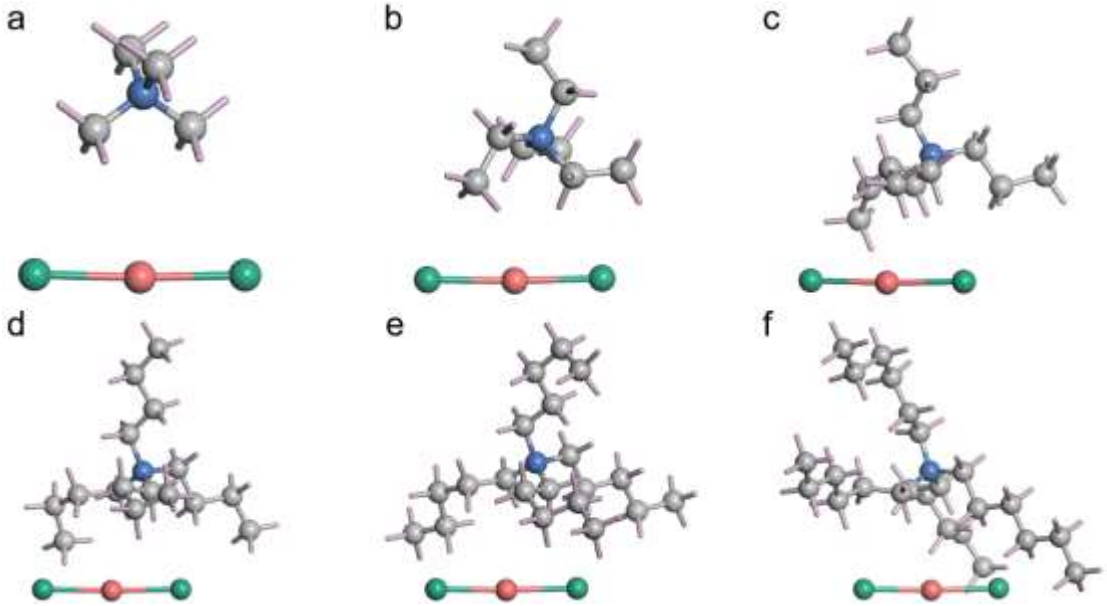

Figure S1 | The structural of quaternary ammonium dichloroiodates ($QICl_2$).

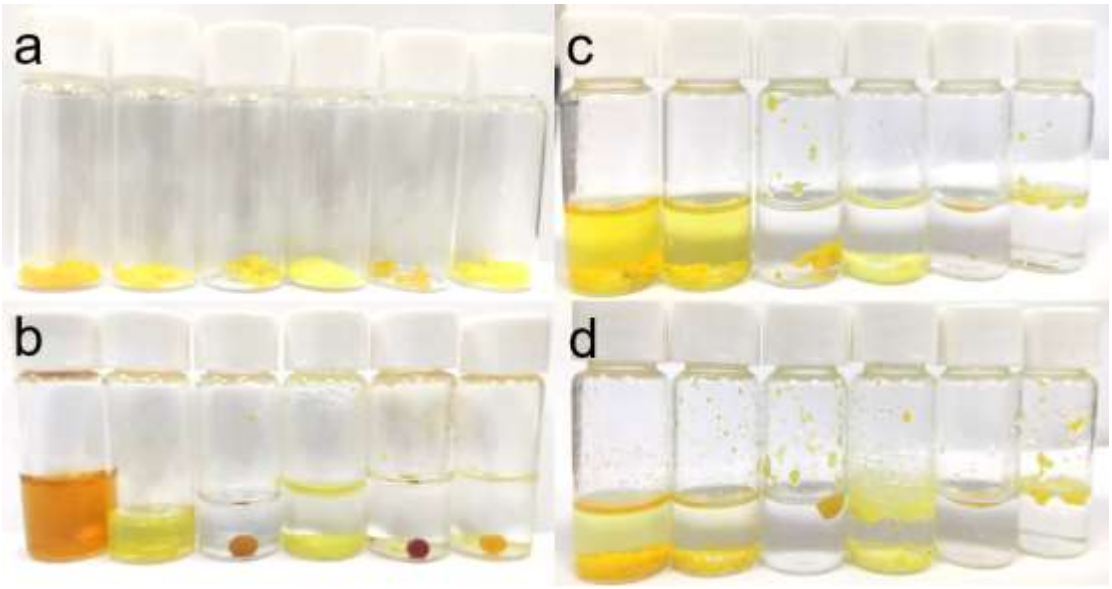

Figure S2 | Digital photo of equimolar of $QICl_2$ in different environments (from left to right is Me_4NICl_2, Et_4NICl_2, Pr_4NICl_2, Bu_4NICl_2, Amy_4NICl_2, $Hexy_4NICl_2$). **a**, air, **b**, H_2O, **c**, 1 m $ZnSO_4$ + 1m $ZnCl_2$ and **d**, 3 m $ZnSO_4$ + 1m $ZnCl_2$. **a**,**c**,**d**, were taken after sample standing a week for its' stable while **b**, was taken after sample standing for 6 months.

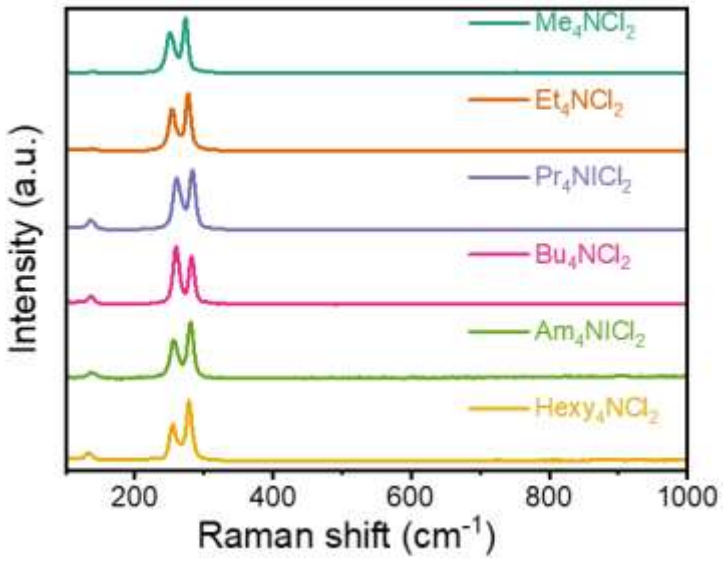

Figure S3 | The Raman spectra of $QICl_2$ compounds in range of 100-1000 cm^{-1}.

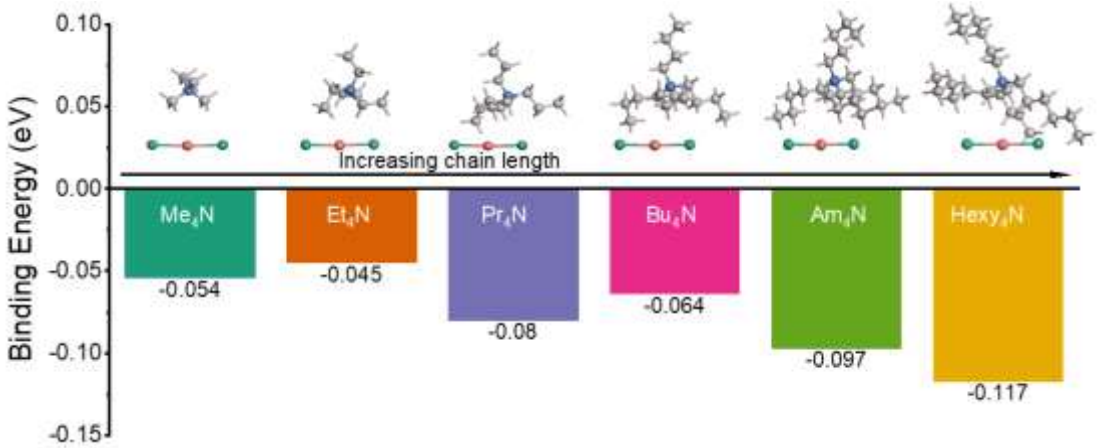

Figure S4 | The calculated binding energy of quaternary ammonium cations with ICl_2^- in aqueous media.

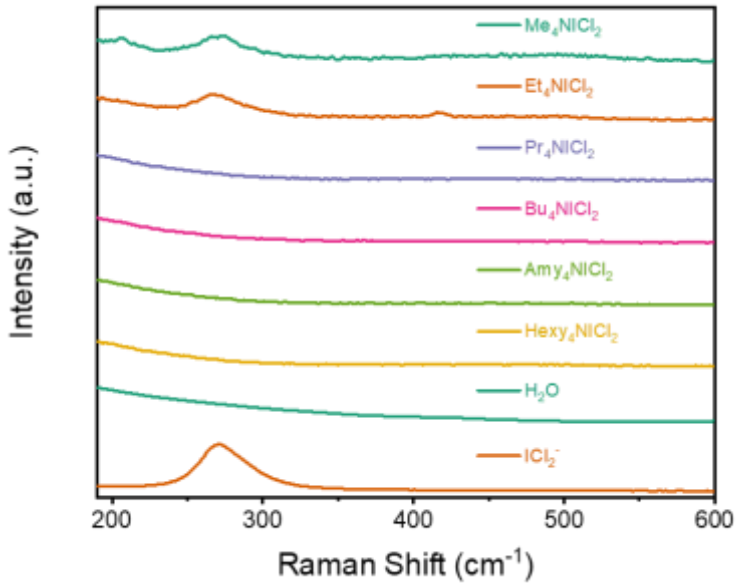

Figure S5 | The Raman spectra of water, and $HICl_2$ solution (prepared by mixing HIO_3 and HCl solution) and the solution of $QICl_2$ compounds in water related to **Figure S2b.**

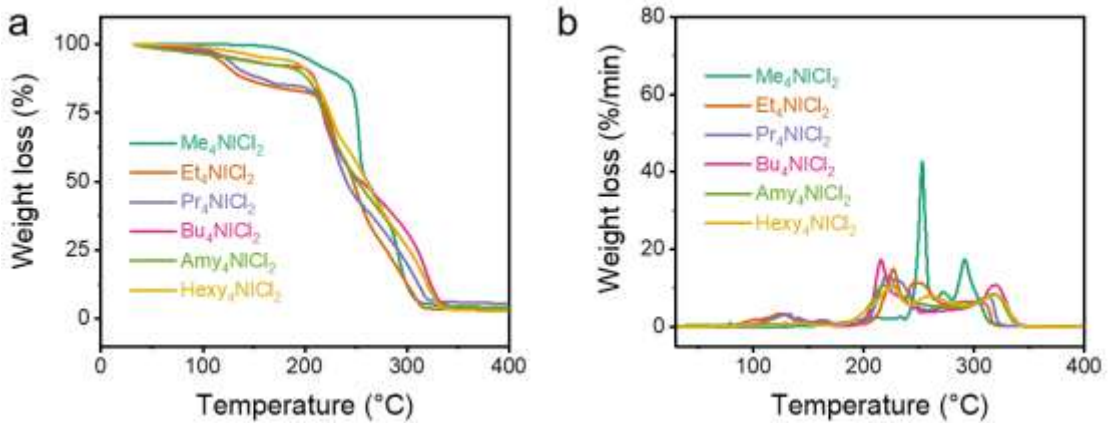

Figure S6 | **a,** The Thermogravimetric analysis curves and **b,** associated differential thermal analysis curves of $QICl_2$ compounds.

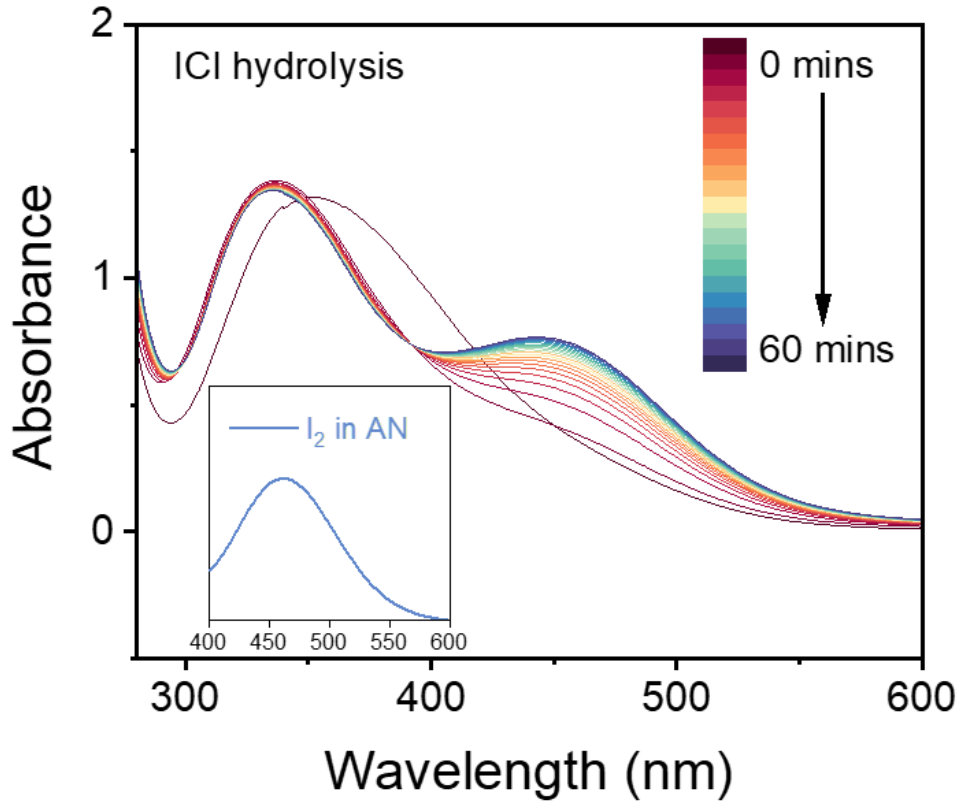

Figure S7 | UV-vis spectra of ICl in acetonitrile solution verst time after addition of 10 vol% H_2O. Insert, the UV-vis spectra of iodine in acetonitrile solution.

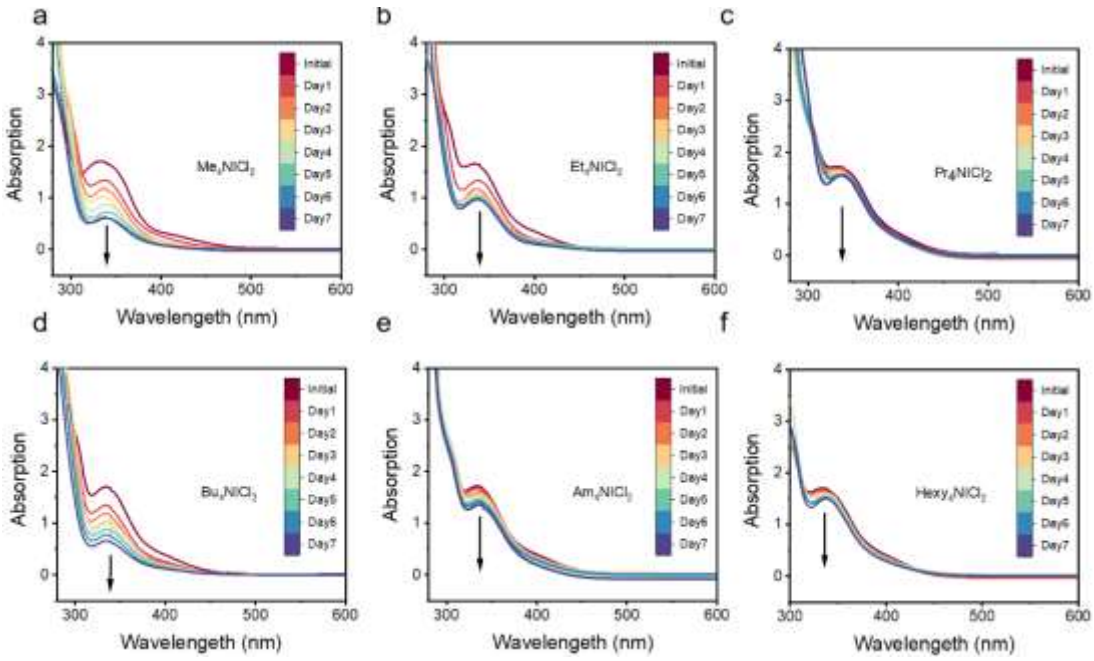

Figure S8 | UV-vis spectra of $QICl_2$ compounds before and after H_2O attack with different times.

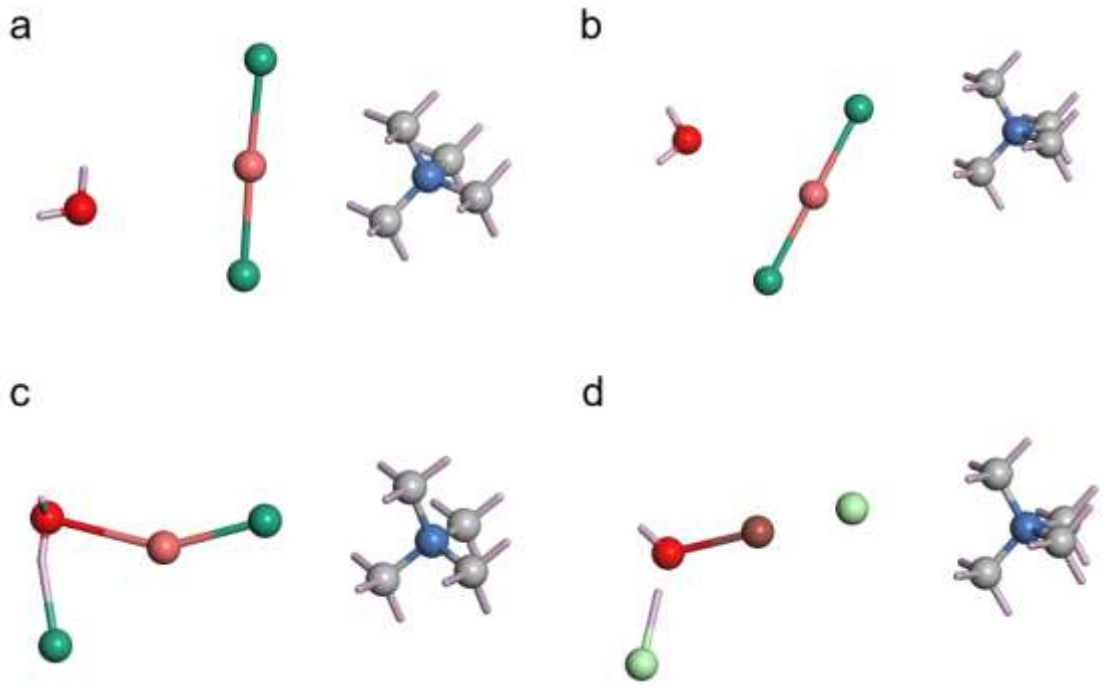

Figure S9 | **a)** Initial state, **b, c)** transition state and **d)** final state of Me_4NICl_2 hydrolysis process.

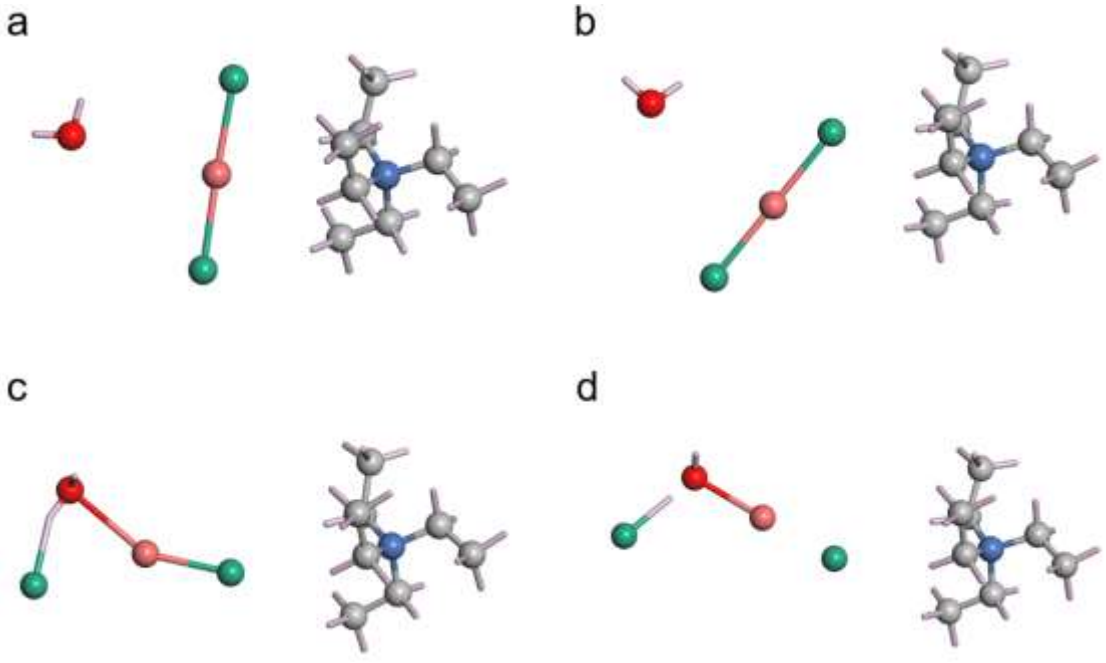

Figure S10 | **a)** Initial state, **b, c)** transition state and **d)** final state of Et_4NICl_2 hydrolysis process.

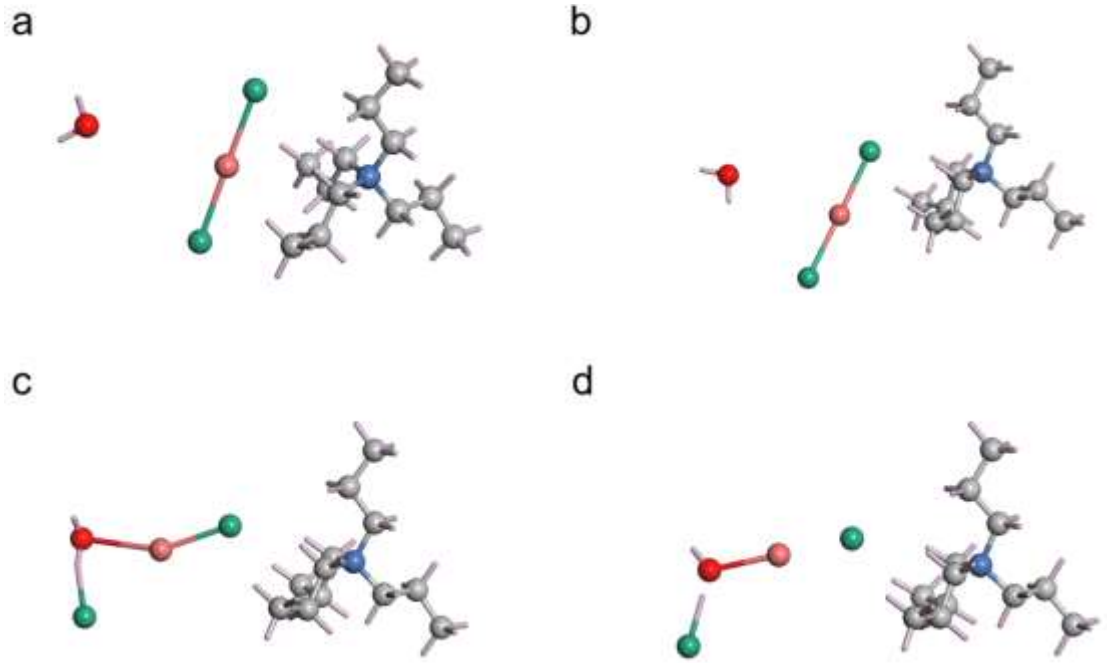

Figure S11 | **a)** Initial state, **b, c)** transition state and **d)** final state of Pr_4NICl_2 hydrolysis process.

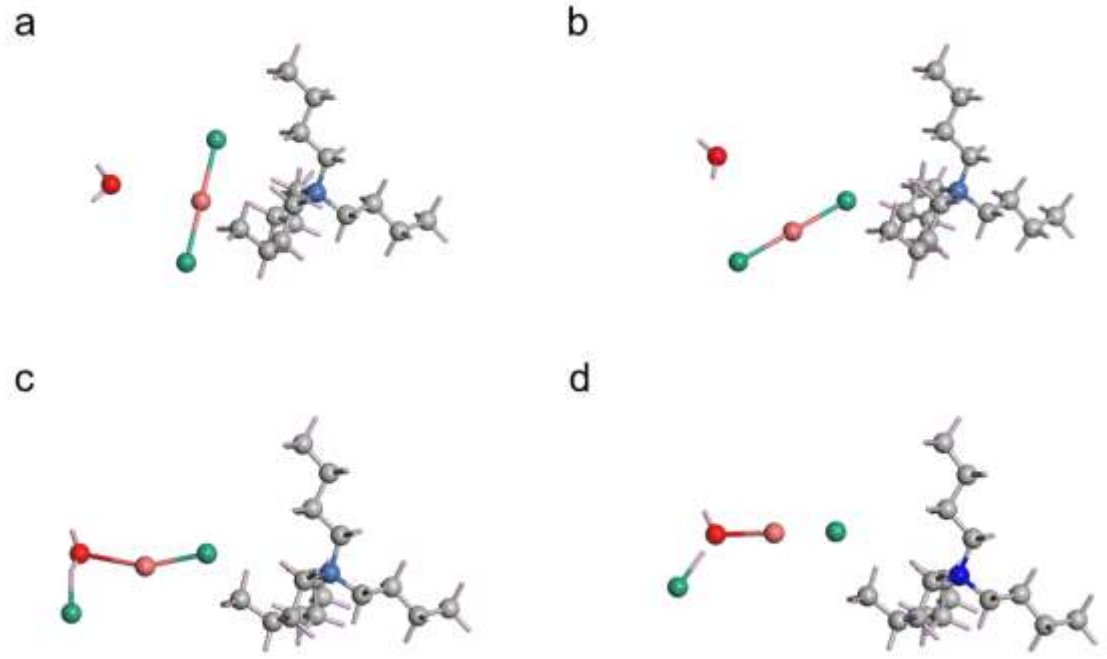

Figure S12 | **a)** initial state, **b, c)** transition state and **d)** final state of Bu_4NICl_2 hydrolysis process.

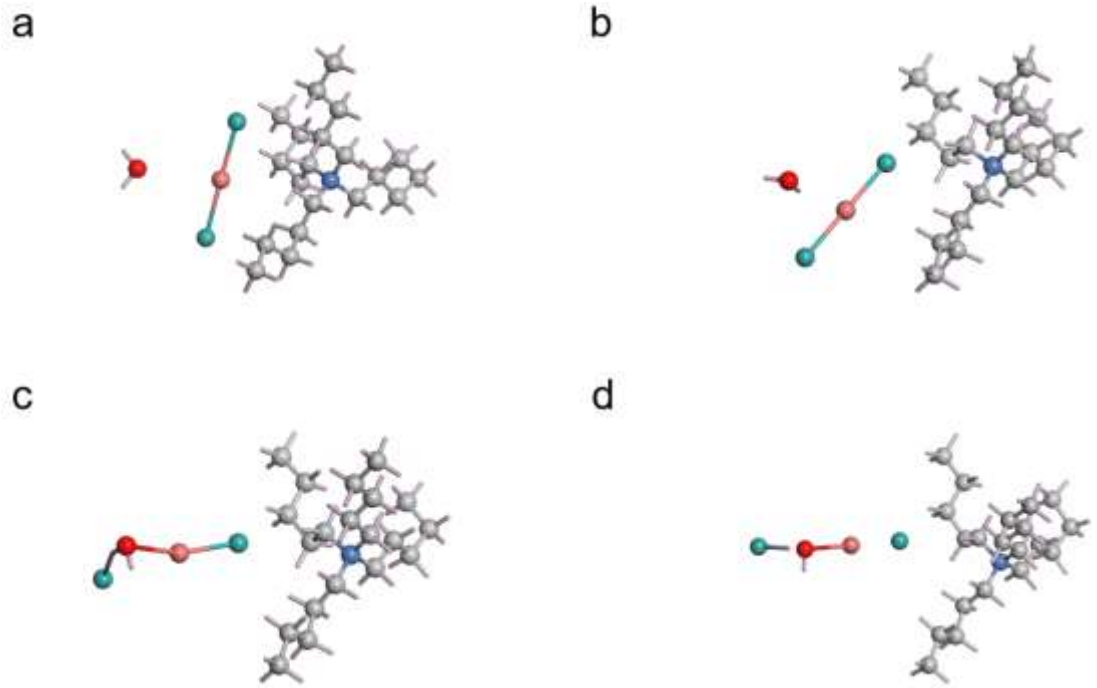

Figure S13 | **a)** initial state, **b, c)** transition state and **d)** final state of Am_4NICl_2 hydrolysis process.

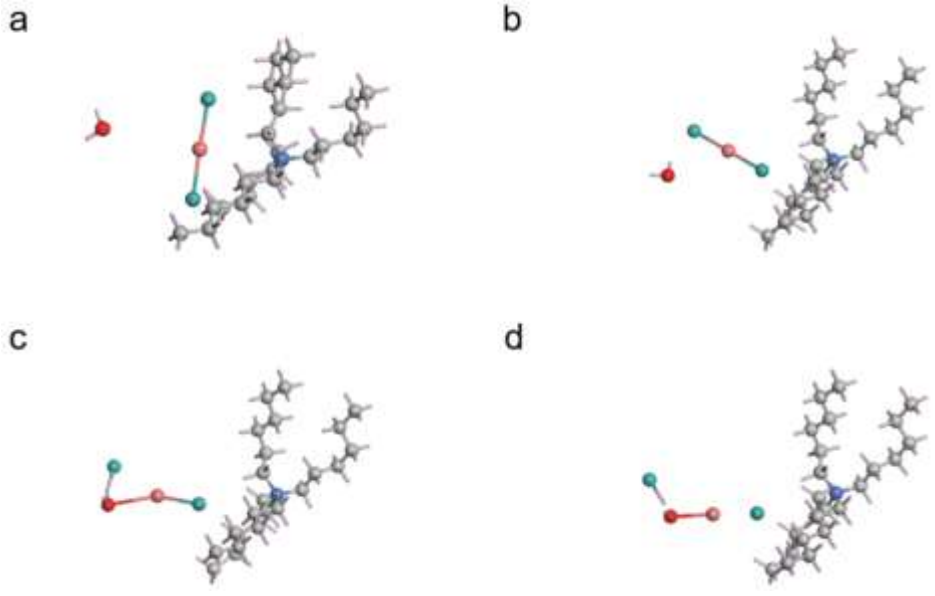

Figure S14 | **a)** initial state, **b, c)** transition state and **d)** final state of $Hexy_4NICl_2$ hydrolysis process.

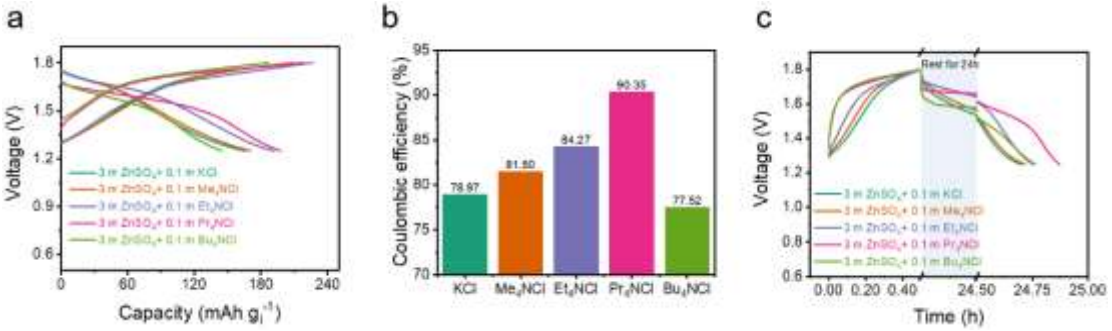

Figure S15| Zinc-iodine batteries with different electrolytes in voltage range of 1.25-1.8 V. **a,** Voltage profile and **b,** coulombic efficiency of zinc-iodine battery in 1.25 V-1.8 V. **c**, Voltage profiles with 6 hours resting time of the Zinc-iodine batteries.

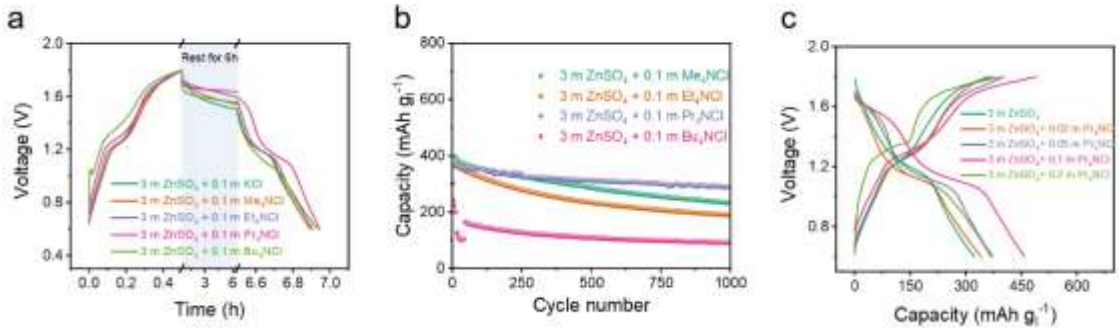

Figure S16| Zinc-iodine batteries with different electrolytes in voltage range of 0.6-1.8 V. **a**, Voltage profiles with 6 hours of rest between charge and discharge processes. **c,** Long-term cycle behaviors of batteries with different electrolytes. **d**, Typical charge/discharge profile of zinc-iodine batteries with various concentration of Pr_4NCl additive in 0.6 V-1.8 V.

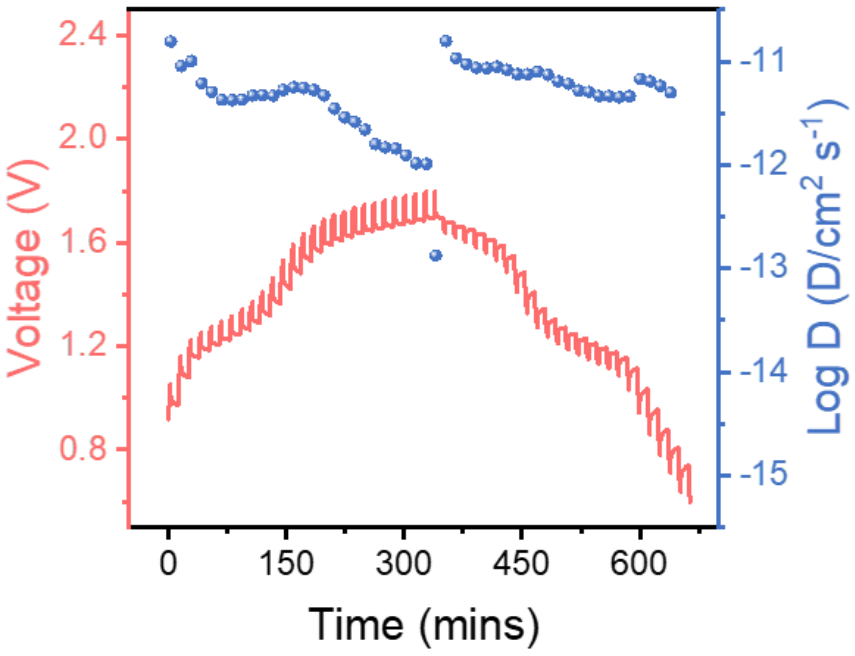

Figure S17 | GITT profile and the diffusion coefficient during charge/discharge process.

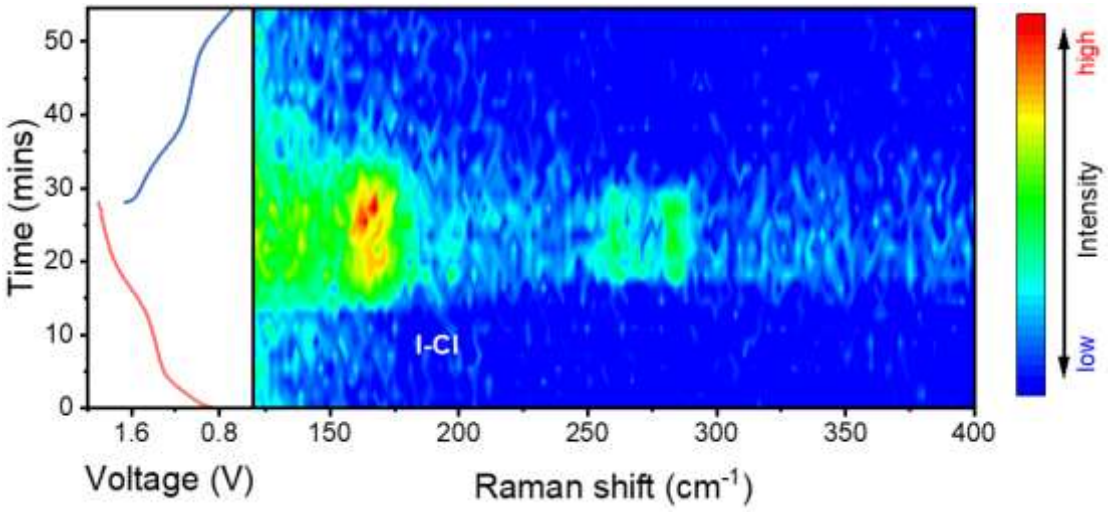

Figure S18 | In-situ Raman spectrum of Zinc-iodine battery with electrolyte of 3 m $ZnSO_4$ + 0.1 m Pr_4NCl during charge/discharge process.

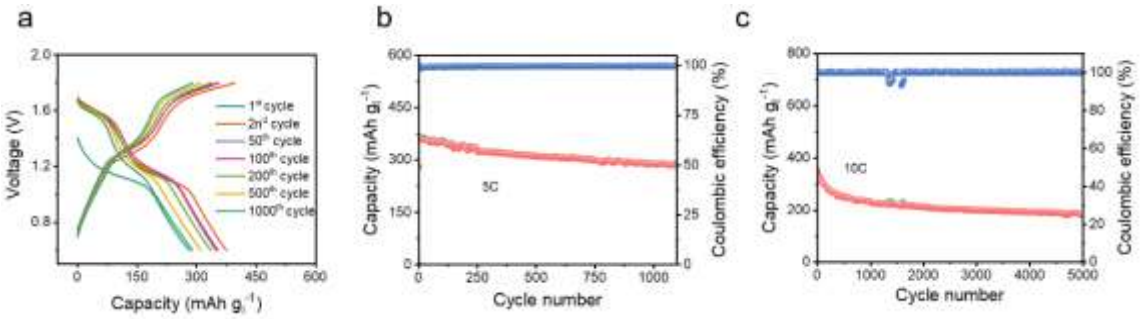

Figure S19 | **a**, Voltage profile of Zinc-iodine batteries at 5C. Long-time cycle performance of 3 m $ZnSO_4$ + 0.1 m Pr_4NCl at **b**, 5C and **c**, 10C

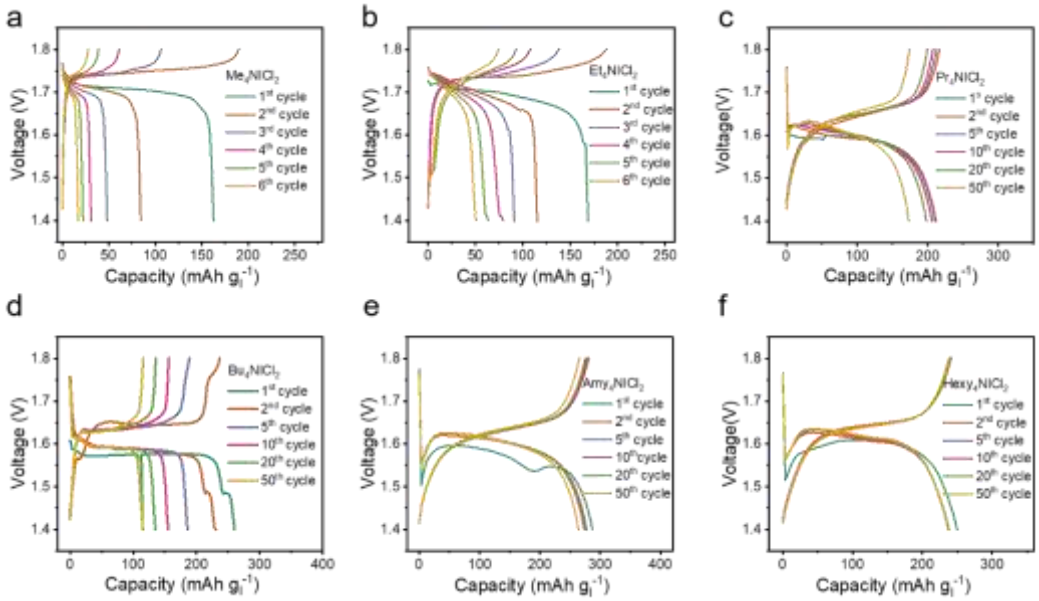

Figure S20 | Voltage profile of **a,** Me_4NICl_2, **b,** Et_4NICl_2, **c,** Pr_4NICl_2, **d,** Bu_4NICl_2, **e,** Amy_4NICl_2, **f,** $Hexy_4NICl_2$ in 3 m $ZnSO_4$+1 m $ZnCl_2$.

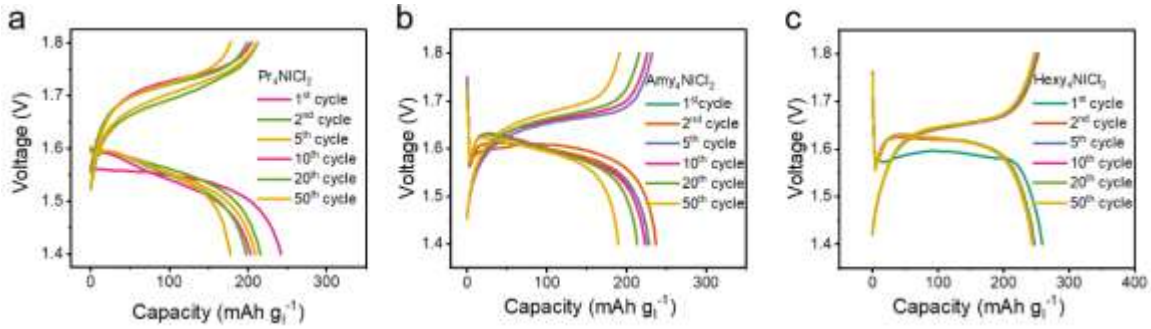

Figure S21 | Voltage profile of **a** Pr_4NICl_2, **b** Amy_4NICl_2, **c** $Hexy_4NICl_2$ in 1 m

$ZnSO_4$+1 m$ZnCl_2$.

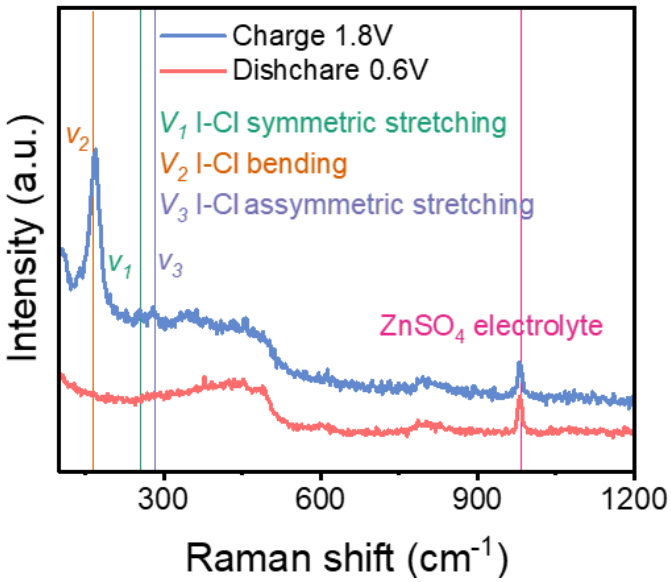

Figure S22 | Specific Raman profile of $Hexy_4NICl_2$ cathode at 1.8 V and 0.6 V corresponding to **Figure 4b**.

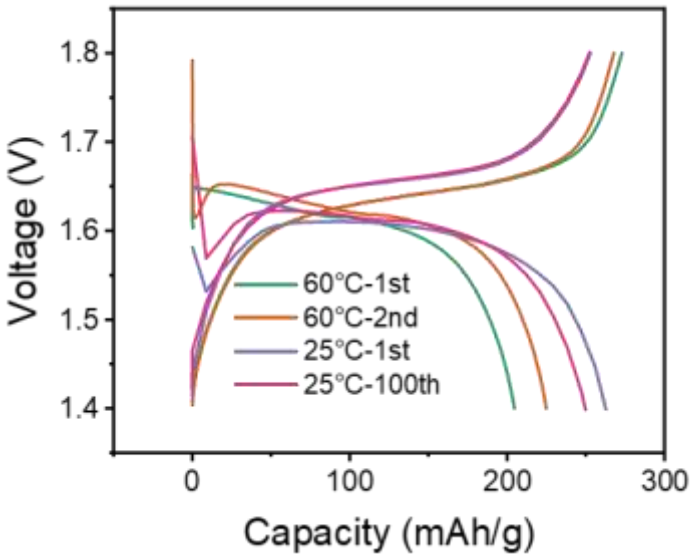

Figure S23 | Voltage profile of $Hexy_4NICl_2$ cathode with different temperature.

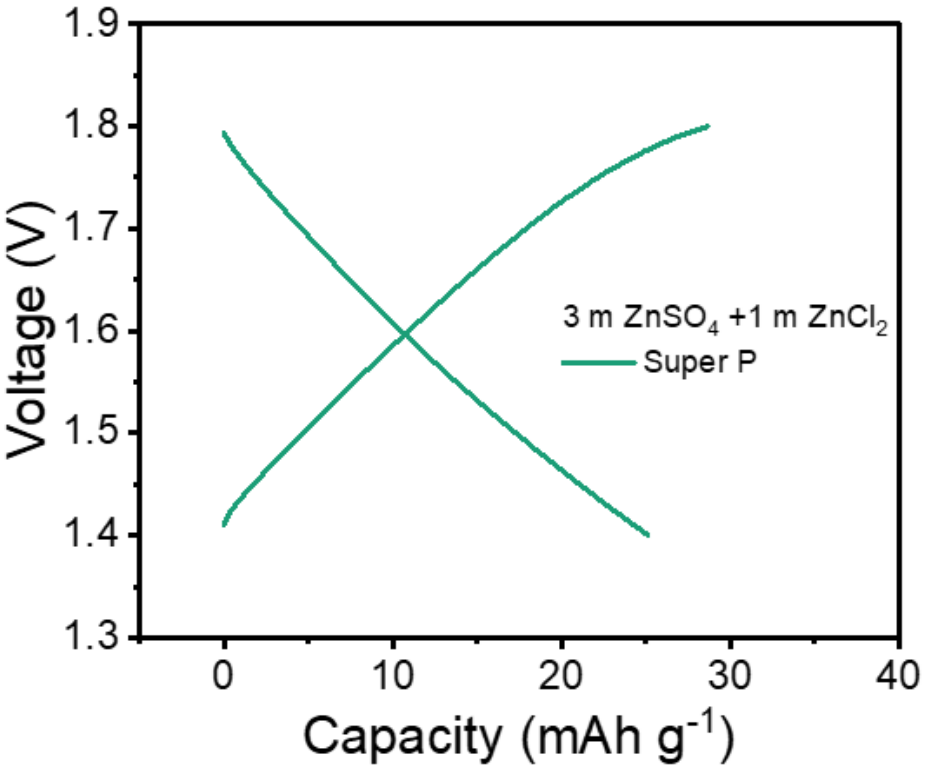

Figure 24| Voltage profile of the cell using 3 m $ZnSO_4$ + 1 m $ZnCl_2$ solution as electrolyte, Zinc anode and super P cathode.

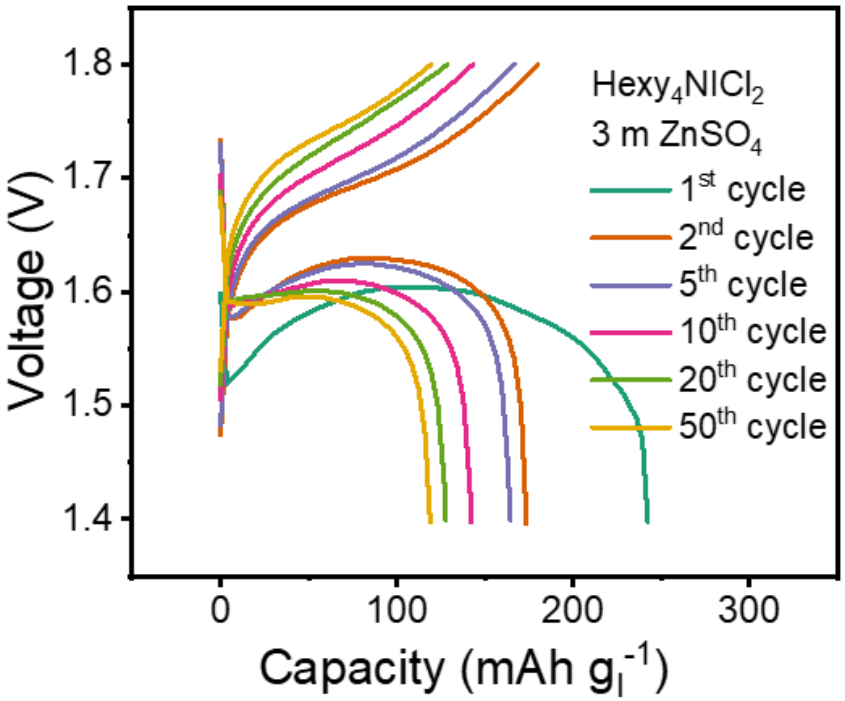

Figure S25 | Voltage profile of $Hexy_4NICl_2$ in electrolyte of 3 m $ZnSO_4$.

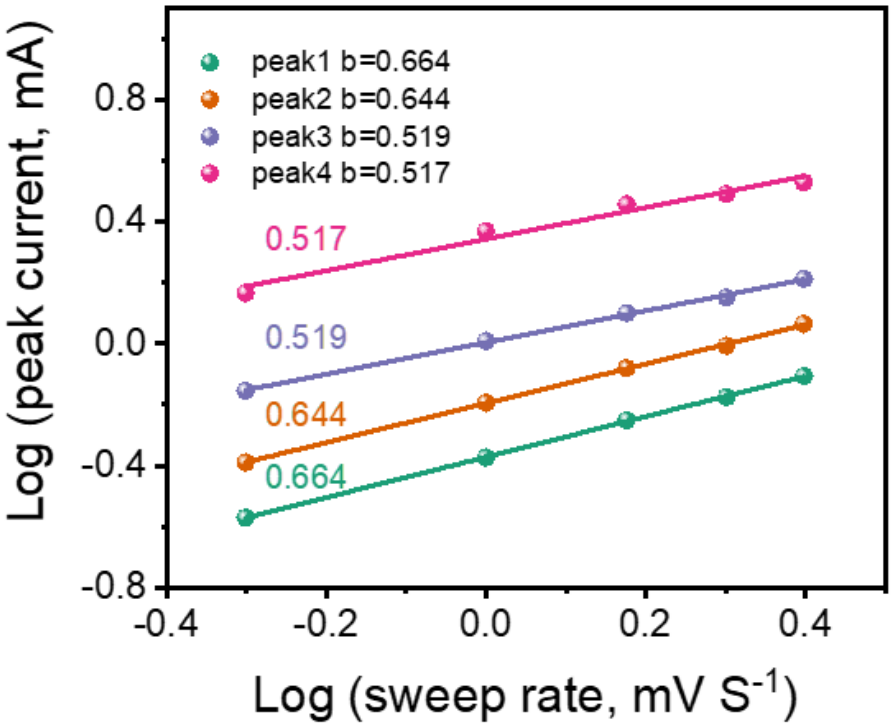

Figure S26| The line relationship of Log (i) vs log (v) at the oxidation and reduction peaks of $Hexy_4NICl_2$ with 3 m $ZnSO_4$+ 1 m $ZnCl_2$.

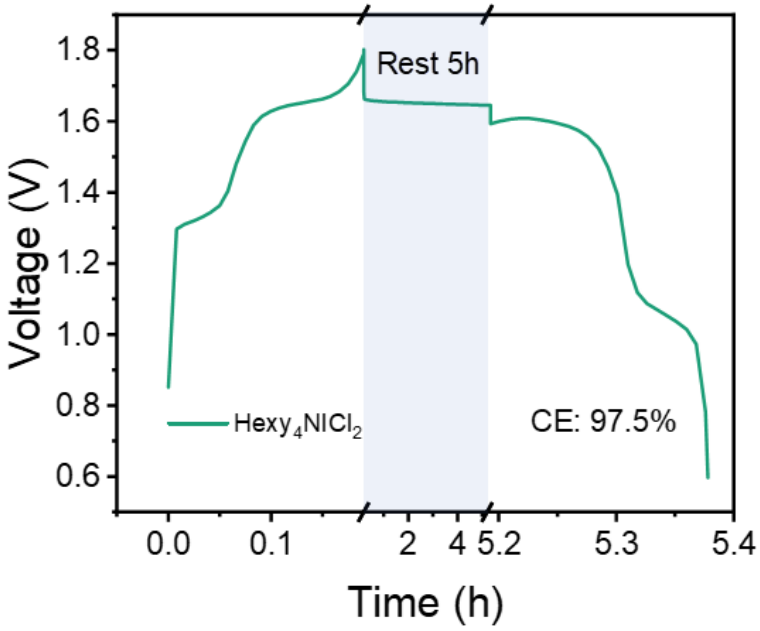

Figure S27| Voltage profiles with 5 hours of rest between charge and discharge processes of zinc-iodine battery using $Hexy_4NICl_2$ cathode in voltage range of 0.6-1.8 V.

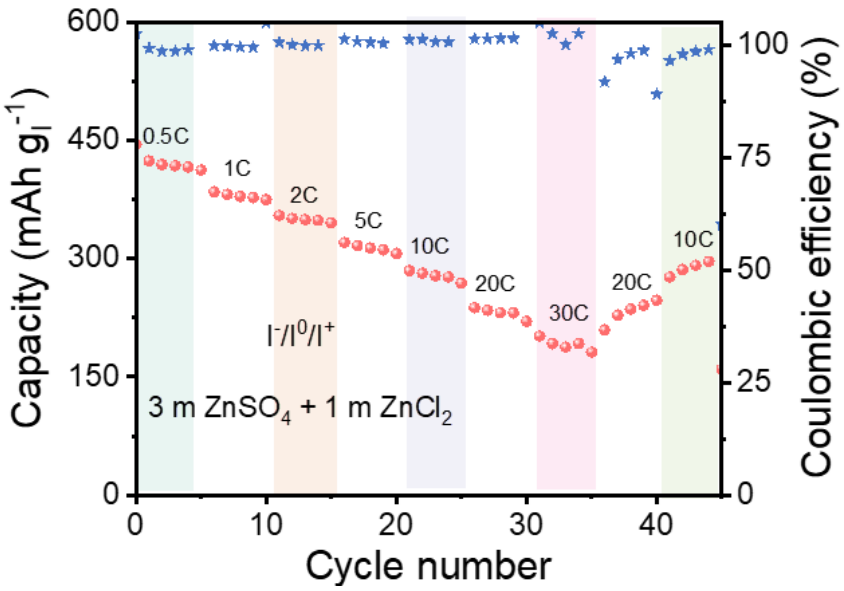

Figure S28| Rate performances of $Hexy_4NICl_2$ cathode with 3 m $ZnSO_4$+1 m $ZnCl_2$.

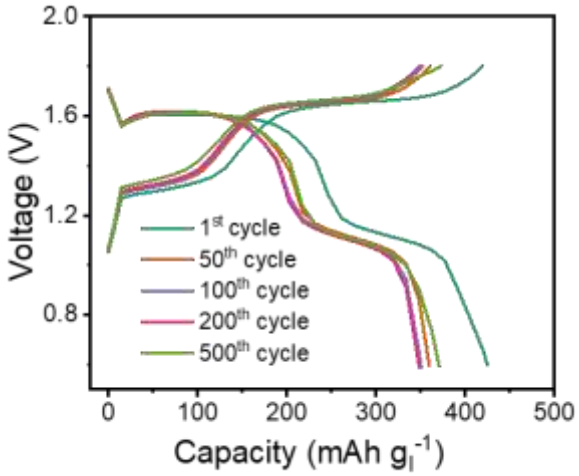

Figure S29| Voltage of $Hexy_4NICl_2$ cathode at 5C with electrolyte of 3 m $ZnSO_4$+1 m $ZnCl_2$.

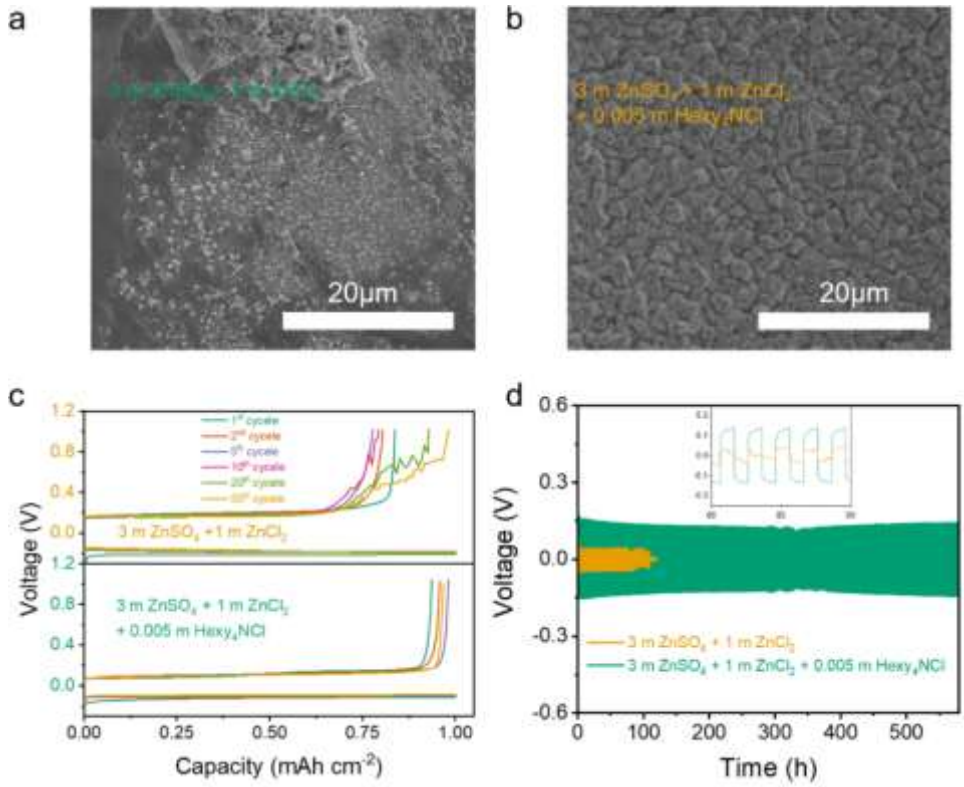

Figure S30 | Characterization and electrochemical performance of the Zn anode. **a, b** SEM images of the Zn electrodes cycled for 1 h at 1 mA cm^{-2} in 3 m $ZnSO_4$ + 1 m $ZnCl_2$ and 3 m $ZnSO_4$ + 1 m $ZnCl_2$ + 0.005 m $Hexy_4NCl$, respectively. **c**, Voltage profile of zinc plating/stripping on Ti foil (1 mA cm^{-2}, 1 h for the plating). **d**, the plating/stripping in Zn||Zn symmetric cells at 1 mA cm^{-2} and 1 mAh cm^{-2}.

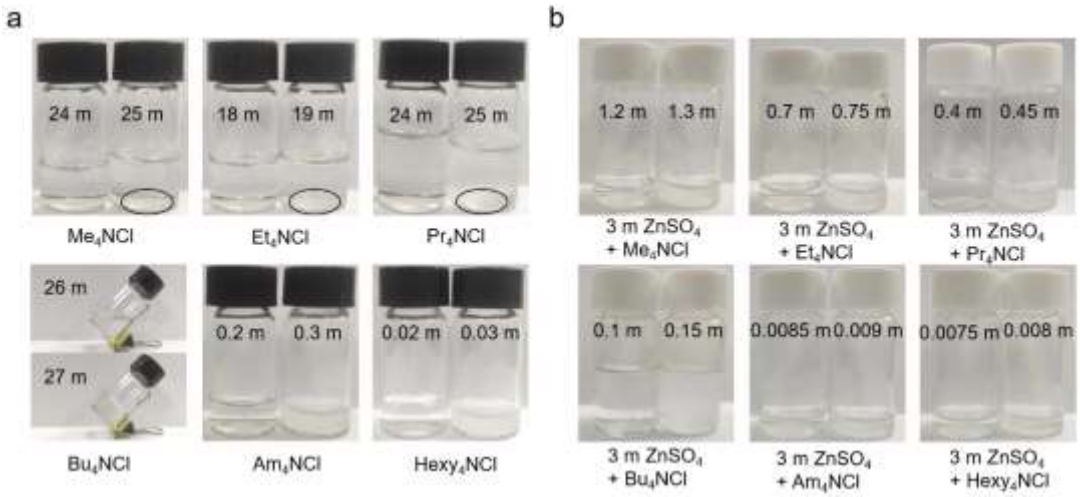

Figure S31 | The picture of the prepared solutions to the determine the solubility of quaternary ammonium chlorides in **a**, H_2O and **b**, 3 m $ZnSO_4$. (In each pair of image comparisons, the left one is clear and the right one has precipitates (mark with circle) or in cloudy suspension. (Related to Supplementary Table 1)

Supplementary Table 1 Solubility of quaternary ammonium chlorides in H_2O and 3 m $ZnSO_4$.

Salt	Me_4NCl	Et_4NCl	Pr_4NCl	Bu_4NCl	Am_4NCl	$Hexy_4NCl$
H_2O	24	18	24	26	0.2	0.02
3m $ZnSO_4$	1.2	0.7	0.4	0.1	0.0085	0.0075

Supplementary Table 2 Price of some Zn-salts and solvents

Salt/Solvent	$ZnSO_4$	$ZnCl_2$	Pr_4NCl	LiCl	AN	H_2O
Price ($ kg^{-1})	43	82	983	202	36	0.1

Price information on these salts and solvents was mainly taken from Aladdin reagent suppliers (https://www.aladdin-e.com) on 5 May, 2023.

Supplementary Table 3 Price of some Electrolytes

Electrolyte	3 m $ZnSO_4$ + 0.1 m Pr_4NCl	19 m $ZnCl_2$ + 19 m LiCl + 8 m AN	30 m $ZnCl_2$	3 m $ZnSO_4$
Price ($ kg^{-1})	28.4	81.9	62.0	14.1

The price of these electrolytes is calculated based on the price of salts and solvents provided in Supplementary Table 2.